Colloidal CuInSe2 Nanocrystals in the Quantum Confinement Regime: Synthesis, Optical Properties, and Electroluminescence

ARTICLE *in* THE JOURNAL OF PHYSICAL CHEMISTRY C · JUNE 2011

Impact Factor: 4.77 · DOI: 10.1021/jp204249j

6 AUTHORS, INCLUDING:

Haizheng Zhong
Beijing Institute of Technology
68 PUBLICATIONS **1,889** CITATIONS

SEE PROFILE

Enrico Bovero
University of Victoria
25 PUBLICATIONS **463** CITATIONS

SEE PROFILE

THE JOURNAL OF PHYSICAL CHEMISTRY C

ARTICLE

pubs.acs.org/JPCC

Colloidal $CuInSe_2$ Nanocrystals in the Quantum Confinement Regime: Synthesis, Optical Properties, and Electroluminescence

Haizheng Zhong,*,† Zhibin Wang,§ Enrico Bovero,⊥ Zhenghong Lu,§ Frank C. J. M. van Veggel,⊥ and Gregory D. Scholes*,‡

†School of Materials Science and Engineering, 5 Zhongguancun South Street, Beijing Institute of Technology, Beijing 100081, China

‡Department of Chemistry, Institute for Optical Sciences, and Centre for Quantum Information and Quantum Control, 80 St. George Street, University of Toronto, Toronto, Ontario M5S 3E4, Canada

§Department of Materials Science and Engineering, 184 College Street, University of Toronto, Toronto, Ontario M5S 3E4, Canada

⊥Department of Chemistry, University of Victoria, P.O. Box 3065, Victoria, British Columbia V8W 3V6, Canada

Supporting Information

ABSTRACT: Photoluminescent, near-stoichiometric colloidal $CuInSe_2$ nanocrystals are synthesized in large batches and with good colloidal quality. An organometallic method is used with a moderate reaction temperature (≤200 °C) to produce $CuInSe_2$ nanocrystals with size-tunable photoluminescence spectra ranging from ~600 to ~850 nm. Two-dimensional photoluminescence excitation−emission maps are reported for the $CuInSe_2$ nanocrystals, highlighting the size-tunable excitonic features. Type I heterostructured $CuInSe_2$/ZnS nanocrystals are prepared and purified. They are found to have absolute photoluminescence quantum yields up to ~26%. The potential to use $CuInSe_2$/ZnS core/shell nanocrystals as a potential low toxicity active layer in light-emitting diodes is demonstrated by fabricating electroluminescent devices.

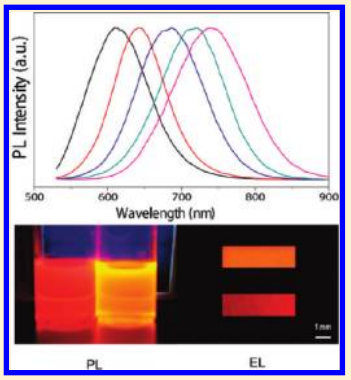

1. INTRODUCTION

Colloidal semiconductor nanocrystals (NCs) are receiving considerable attention due to their size-tunable spectroscopic properties[1] and their applications as light-emitters or solar-harvesters in optical and electronic devices.[2−7] As light-emitting and solar-harvesting materials, semiconductor NCs offer several notable properties that, in combination, can be advantageous compared to their bulk counterparts and organic molecules: (1) the absorption and emission spectra can be tuned by varying their size, shape, and structure; (2) as light emitters, they have high photoluminescence (PL) emission quantum yields (QYs) with good photostability; (3) semiconductor NCs in the quantum confinement regime have potential to utilize carrier multiplication and hot carriers, which may improve device applications.[8,9] However, the exploration of NC applications has mainly focused on cadmium- and lead-based NCs, which have a doubtful future because of their high toxicity. A current challenge is to move away from toxic materials and turn to more environmental friendly semiconductor NCs.[10]

I−III−VI semiconductors, such as $CuInS_2$, $CuInSe_2$, and $AgInS_2$, have been identified as candidates for low toxicity light-emitters and solar-harvesters.[11−13] Of particular interest, $CuInSe_2$ has the lowest direct band gap of ~1.04 eV and large calculated exciton Bohr radius of ~10.6 nm, and the bulk material has excellent photovoltaic performance.[14] In recent work $CuInSe_2$ NCs were studied as solar-harvesters for solution-processed solar cells.[15,16] Furthermore, $CuInSe_2$ NCs in the strong quantum confinement regime ($d \ll 2a_B$, d is the diameter of NC, a_B is exciton Bohr radius) are predicted to be luminescent emitters in the red and near-infrared region.[11] Inspired by these motivations, the synthesis of $CuInSe_2$ NCs has extensively been studied, providing several approaches including single-precursor decomposition,[14] hot injection,[15−20] hydrothermal method,[21,22] and microwave-assisted synthesis.[23,24] In the present work, we report a simple, large-scale, reproducible method to synthesize $CuInSe_2$ NCs through reaction between Cu−In−S_x−R and tri-*n*-butylphosphine selenium (TBPSe) at moderate temperature (≤200 °C).

Although there has been significant progress in the preparation and study of $CuInSe_2$ NCs, there are still many unresolved issues. For example, high quality $CuInSe_2$ NCs can be prepared by using oleylamine as a ligand, but rapid oxidation of the resulting NCs highlights stability issues.[19] Luminescent $CuInSe_2$ NCs have recently been prepared, but to date their photoluminescence properties have not deeply been characterized;[25,26] strong quantum confinement effects

Received: May 6, 2011
Revised: May 31, 2011
Published: June 01, 2011

have not clearly been demonstrated. Bawendi et al. synthesized nonstoichiometric Cu−In−Se NCs with red to near-infrared PL emission using bis(trimethylsilyl selenide) precursor (280−360 °C).[25] Omata et al. obtained $CuInSe_2$ quantum dots at 320 °C and investigated their near-infrared PL emission.[26] Very recently, Pons et al. further refined the reaction to prepare emissive Cu−In−Se NCs by using selenourea as selenium precursor.[27] However, controlling the composition and size of ternary NCs is a great challenge. It is therefore desirable to further develop new synthetic methods, which motivated the present study.

The $CuInSe_2$ NCs we report here exhibit PL emission in the red and near-infrared region ranging from ∼600 to ∼850 nm. They have nearly stoichiometric composition and good size control (∼3.4 ± 0.5 nm) in the strong confinement regime. $CuInSe_2$/ZnS core shell materials were prepared and the PL emission was found to be greatly enhanced by the ZnS shell. Two-dimensional photoluminescence excitation−emission maps (2D-PLE) were used to investigate the excitonic properties of the NCs. We also explored the applications of $CuInSe_2$/ZnS NCs in electroluminescence devices. These initial results of light-emitting devices based on I−III−VI NCs demonstrate the potential of $CuInSe_2$-based NCs in light-emitting diodes (LEDs).

2. EXPERIMENTAL SECTION

Chemicals. All manipulations were carried out using standard Schlenk line technique under dry argon. Copper(I) iodide (Fluka, ≥ 98%), indium(III) acetate (Aldrich, 99.999%), zinc stearate ($Zn(St)_2$, Alfa Aesar), selenium (Aldrich, 100 mesh, 99.5%,), *n*-dodecanethiol (DDT, Alrich, ≥98%), *n*-octadecanethiol (ODT, Aldrich, 90%), oleic acid (OA, Aldrich, 90%), tri-*n*-butylphosphine (TBP, Alrich, 97%), tri-*n*-octylphosphine (TOP, Alrich, 90%), and 1-octadecene (ODE, Aldrich, 90%) were used as purchased and without further purification.

Synthesis of $CuInSe_2$ NCs. A typical synthesis of $CuInSe_2$ nanocrystals was performed as follows: CuI (96 mg, 0.5 mmol) and $In(OAc)_3$ (146 mg, 0.5 mmol) were mixed with 0.5 mL of dodecanethiol and 10 mL of ODE in a 25 mL three-necked flask. The mixture was degassed at 120 °C for 30 min, then 0.5 mL of oleic acid was added into the solution, and the solution was continuously degassed for another 30 min. After that, the solution was heated to 200 °C under argon flow, and 1 mL of TBPSe precursor (made by dissolving 1 mmol of Se powder in 0.25 mL of TBP and 0.75 mL of ODE) was swiftly injected into the flask and kept for a fixed time at the same temperature. During the reaction, aliquots were taken via syringe at different times to monitor the growth of $CuInSe_2$ NCs by recording UV−vis and PL spectra. Afterward, the reaction solution was cooled to room temperature and precipitated by acetone, the flocculent precipitate formed was centrifuged, the upper layer liquid was decanted, and then the isolated solid was dispersed in chloroform and reprecipitated by adding menthol or acetone. The centrifugation and precipitation procedure was repeated several times for purification of the prepared $CuInSe_2$ nanocrystals. Finally, the final products were redispersed into toluene or chloroform or dried under vacuum for measurements. Typically, one batch experimental can produce ∼120 mg of $CuInSe_2$ NCs powder.

Synthesis of $CuInSe_2$/ZnS NCs. The as-prepared $CuInSe_2$ NCs were separated from the reaction solution by acetone. Without further purification, half of the as-prepared $CuInSe_2$ NCs were transferred to another flask containing 20 mL of ODE. Then 0.5 mmol (0.32 g) of $Zn(St)_2$ was added into the solution, and the whole solution was purged with argon and degassed at 120 °C to remove any low boiling point chemicals. After that, the solution was heated to 200 °C, and 1 mL of *n*-dodecanethiol was separately added into the solution in 60 min to grow the ZnS shell.

Material Characterization. Transmission electron microscopy (TEM) and high-resolution transmission electron microscopy (HR-TEM) images were recorded using a JEOL-2100F instrument equipped with a Gatan camera operated at 200 kV. Scanning transmission electron microscopy (STEM) images were acquired using a Hitachi HD-2000 at 200 kV. Energy-dispersive X-ray spectroscopy (EDS) was performed using Hitachi 5200 equipment with an Oxford Instruments Inca EDS microanalysis system operated at 20 kV. X-ray diffraction (XRD) measurements were carried out on a Siemens D5000 X-ray powder diffractometer using a high-power Cu Kα source operating at 50 kV and 35 mA with a Kevex solid-state detector. A step scan mode was used for data collection with a step size of 0.028 and time of 2.0 s per step.

Optical Characterization. Absorption spectra were obtained on a Varian 100 BIO UV/vis spectrophotometer. Steady-state PL spectra were obtained using a Varian CARY fluorescence spectrometer or Jasco V-570 spectrophotometer. The PL QYs of the samples were determined by the following methods. All the measurements were performed with an "Edinburgh Instruments" FLS 920 fluorimeter. The excitation source was a 450 W Xe arc lamp and the detector an R928P Hamamatsu PMT. The resolution of the measurements was 1 nm determined by the aperture of the slits. The absolute quantum yield was determined measuring emission and scattered light from the sample and reference in an integrating sphere (Edinburgh instruments, 150 mm in diameter coated with barium sulfate). All the samples were dispersed in toluene and placed in a cuvette inside the integrating sphere. The emitted and scattered radiation was collected at a 90° angle from the excitation, and a baffle was placed beside the sample on the emission monochromator side to avoid the collection of directly scattered light. The formula used to calculate the quantum yield was

$$\mathrm{QY} = \frac{\int I_{\mathrm{E}}(\bar{\nu})\,\mathrm{d}\bar{\nu}}{\int I_{\mathrm{S-C}}(\bar{\nu}) - \int I_{\mathrm{S-S}}(\bar{\nu})\,\mathrm{d}\bar{\nu}} \qquad (1)$$

Here, QY is the quantum yield, I_{E} is the emission intensity, $I_{\mathrm{S-C}}$ and $I_{\mathrm{S-S}}$ are the intensities of the radiation scattered from the reference sample and from the sample, respectively. $\bar{\nu}$ denotes frequency in wavenumbers. The reference sample consisted of just toluene. The reported results were obtained using excitation at 420 nm, and control experiments at 380 nm excitation found the same results.

Device Fabrication. All the devices were fabricated on commercially line-patterned indium tin oxide (ITO) coated glass having a sheet resistance of 15 Ω/sq. The width of the ITO lines is 1 mm. Substrates were ultrasonically cleaned with a standard regiment of Alconox, acetone, and methanol for 15 min each, followed by UV ozone treatment for 15 min. 2 mg/mL Poly-TPD [TPD: 4-butylphenyldiphenylamine] in 1,2-dichlorobenzene was spin-coated on the top of the ITO at 2000 rpm

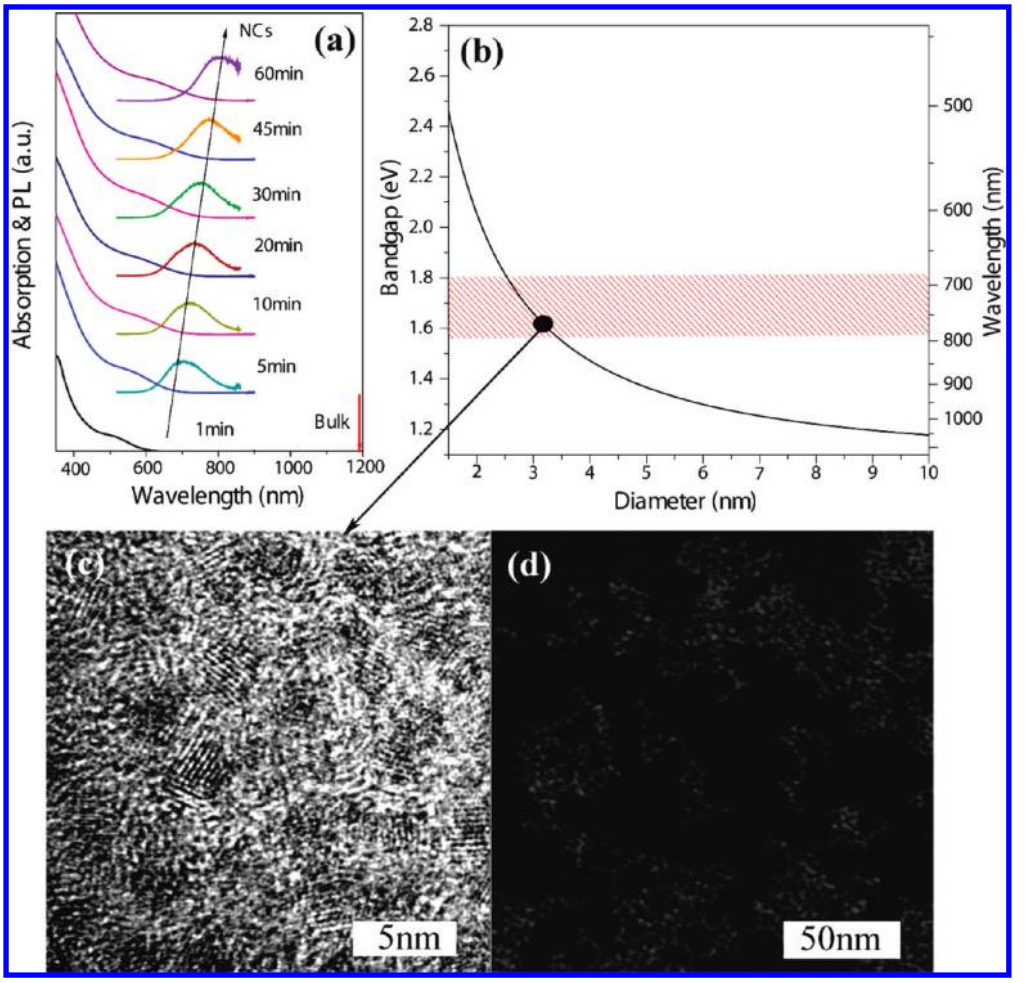

Figure 1. (a) Absorption and PL spectra of $CuInSe_2$ NCs with injection and growth at 200 °C. (b) The size-dependent optical bandgap of $CuInSe_2$ NCs predicted using simple EMA calculations. (c) TEM images of $CuInSe_2$ samples obtained at 200 °C for 60 min. (d) STEM images of $CuInSe_2$ samples obtained at 200 °C for 120 min.

for 60 s in the glovebox. The polymer layers were dried for over 1 h at ~110 °C in the glovebox. QD dispersions in toluene were then spin-coated at 2000 rpm for 60 s on top of the poly-TPD. After a subsequent drying for 1 h at ~70 °C in the glovebox, substrates were loaded into vacuum and degassed for more than 24 h to further remove the solvent. The rest of the device was fabricated in a Kurt J. Lesker LUMINOS cluster tool with a base pressure of 10^{-8} Torr using stainless steel shadow masks. A 50 nm thick TPBi layer was deposited in a dedicated organic chamber followed by a thin layer of LiF (1 nm) in the same chamber. Subsequently, a 100 nm thick Al cathode was deposited in a dedicated metal chamber using a shadow mask with 5 mm wide. The active area of the devices was hence 5 mm^2. The whole deposition procedure was conducted without breaking vacuum; i.e., the sample was transferred through the central distribution chamber with a base pressure of ~10^{-9} Torr. Film thicknesses were monitored using a calibrated quartz crystal microbalance (QCM). Current−voltage (IV) characteristics were measured using an HP4140B pA meter in ambient air. Luminance measurements were taken using a Minolta LS-110 Luminance meter. EL spectra were measured by a USB 2000 miniature fiber-optic spectrometer, which couples a linear CCD-array detector ranging from 350 to 1100 nm.

3. RESULTS AND DISCUSSION

3.1. Synthesis and Characterization of $CuInSe_2$ NCs. Balancing the nucleation and growth processes by choosing suitable precursors and organic ligands or tuning the reaction temperatures has been important for the synthesis of high quality II−VI NCs.[28,29] In ternary NC synthesis, the balancing of the reactivity of two cationic precursors should be further considered to ensure nucleation of the ternary semiconductor crystal,[30] which makes this very challenging work. An alternative route is to incorporate three elements into a single molecular complex and decompose it thermally.[14,31] Zhong et al. have reported such a procedure for preparing $CuInS_2$ NCs by heating a mixture of copper and indium sources with *n*-dodecanethiol.[32] It was demonstrated that an intermediate complex of $CuIn(SC_{12}H_{25})_x$ was formed and then subsequently decomposed into clusters which grew into $CuInS_2$ NCs. This method was recently refined to give high quality pyramidal $CuInS_2$ NCs.[33] In the present work, we reasoned that the intermediate Cu−In−$(S-R)_x$ clusters can react with TBPSe (TBP: tri-*n*-butylphosphine) or TOPSe (TOP: tri-*n*-octylphosphine) to grow $CuInSe_2$ NCs by cleaving Cu−S or In−S bonds.[34] In a typical experiment, a mixture of copper iodide, indium acetate, *n*-dodecanethiol (DDT), oleic acid

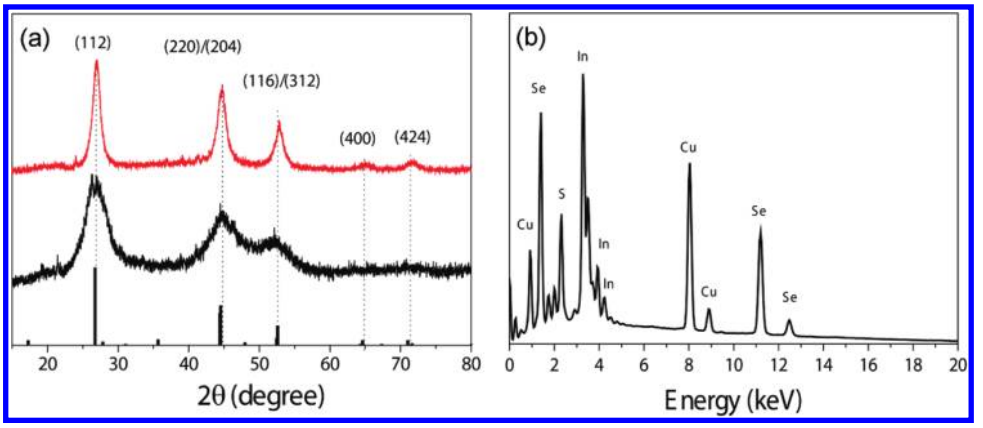

Figure 2. (a) XRD patterns of $CuInSe_2$ NCs prepared at 180 °C (black line) and 200 °C (red line). The XRD pattern for bulk $CuInSe_2$ (black bars, JCPDS 40-1487) is shown as a reference. (b) A typical EDS spectrum of $CuInSe_2$ NCs.

(OA), and octadecene (ODE) was heated to 180−200 °C. Subsequently, TBPSe solution was injected, and the solution was maintained at the injection temperature for growth. After the injection of TBPSe, an immediate color change from light yellow to red was observed in comparison to the slow color change upon continuous heating in the $CuInS_2$ synthesis.

Figure 1a shows the evolution of absorption and PL spectra during typical $CuInSe_2$ NC growth at 200 °C. The absorption and PL spectra of NCs each gradually shift to longer wavelength. Like previous reports, no obvious excitonic absorption peak was observed for the existence of intrinsic and surface trap states.[25,26] The PL spectra are relative broad. Bulk $CuInSe_2$ has a small energy band gap of 1.04 eV (1192 nm) and a large exciton Bohr radius of 10.6 nm, so quantum confinement effects are anticipated for colloidal NCs in the size regime we have prepared. Although there is no marked excitonic band in the absorption spectrum, the size-dependent shifts evident in the spectra—particularly the PL spectrum—suggest quantum confinement of the exciton, as predicted.

Sizes of some of the NC preparations were determined using transmission electron microscopy (TEM) and scanning transmission electron microscopy (STEM). At an early stage of a typical reaction (60 min), the NCs have an average diameter of ~3.4 nm (see Figure 1c and enlarged images in Supporting Information S2). Extending the reaction time to 120 min, the NCs appear as short necklace-like structures with little growth in diameter (see Figure 1d and enlarge images in Supporting Information S2). The necklace structured aggregate is characteristic of oriented attachment, which has been described for CdTe and other systems.[35] We do not examine these structures further here. Finite-depth well effective mass approximation (EMA) theoretical calculations[11] (see Figure 1b; the calculation can be found in the Supporting Information S1) predict based on the PL band energy that the NCs we have prepared have diameters ranging from 2.5 to 3.5 nm.

X-ray diffraction (XRD) patterns (Figure 2a) indicate that the NCs have chalcopyrite (tetragonal) phase structures, which is the stable phase of bulk $CuInSe_2$ at room temperature. Figure 2b presents a typical energy-dispersive X-ray spectroscopy (EDS) spectrum, which confirms the presence of copper, indium, and selenium. Quantitative analysis shows that the elemental composition of $CuInSe_2$ NCs is generally close to the stoichiometric composition (see the Supporting Information S3). A slight

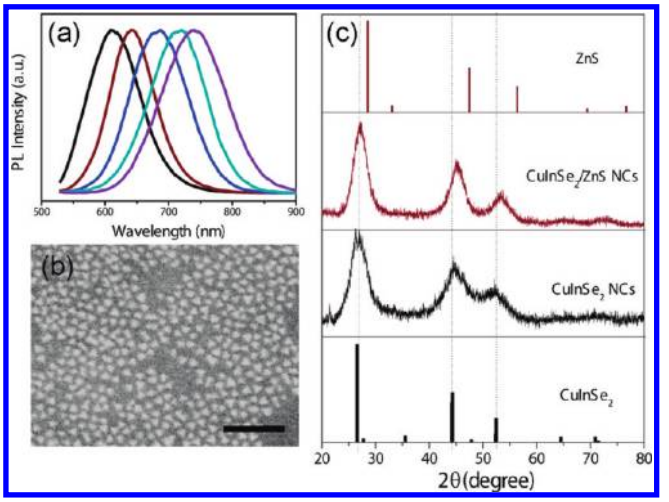

Figure 3. (a) PL spectra of $CuInSe_2$/ZnS core/shell NCs. (b) A representative STEM image of $CuInSe_2$/ZnS core/shell NCs. Scale bar: 25 nm. (c) XRD of $CuInSe_2$ core and $CuInSe_2$/ZnS NCs. The XRD patterns for bulk $CuInSe_2$ (black bars, JCPDS 40-1487) and ZnS (red bars, JCPDS 77-2100) are shown as reference.

deficiency of selenium can be explained by the thiol ligands binding to the NC surface. The Cu/In ratio of the NCs varies from 1:1 to 1:~0.8 by changing their growth temperatures from 180 to 200 °C (see the Supporting Information S3).

Variation of the reaction conditions was further studied. For example, using TOPSe or additional amounts of TBPSe did not produce any obvious change. A multiple injection method was applied to synthesize larger $CuInSe_2$ NCs by slowly adding a mixture of TBPSe and $CuIn(SC_{12}H_{25})_x$. The absorption spectrum was thereby extended from ~760 nm (1.63 eV) to ~950 nm (1.30 eV) (see Supporting Information S4). Alternatively, using ODT as the thiol ligand and changing the reaction temperature to 220 °C enabled the preparation of larger particles (see Supporting Information S4).

3.2. Synthesis and Characterization of $CuInSe_2$/ZnS Core/Shell NCs. Type I core/shell NCs are more suitable for light-emitting applications owing to their greater environmental tolerance and enhanced PL yield.[36] ZnS is a stable wide bandgap shell material suitable to overcoat $CuInSe_2$ NCs. $CuInSe_2$ NCs to serve as cores in the heterostructures were separated from the

reaction system and then transferred to another flask to grow the ZnS shell. The coating process was monitored by using UV−vis and PL spectroscopy. The absorption region ranging from 300 to 350 nm was gradually increased, implying the epitaxial growth of ZnS. The PL emission was obviously enhanced (see Supporting Information S5). The PL peaks of $CuInSe_2$/ZnS NCs shows a 20−50 nm blue shift after coating ZnS shells. Similar observations have been also observed in other reports of coating ZnS shells onto $CuInS_2$ or $CuInSe_2$ NCs.[37−39] The blue shift is quite different from that of general type I CdSe/ZnS or CdSe/CdS core/shell structures, which show a red shift in emission with increasing shell thickness of the particles.[40] The blue shift was attributed to the shrinkage of the effective size of the core $CuInSe_2$ region due to the partial alloying of the core $CuInSe_2$ with the ZnS shell around their interfaces by interdiffusion or surface reconstruction. It is also noted that the emission spectra of some samples have two emission peaks, which are possibly related to the intrinsic and surface trap states.[41]

By using different size cores, the PL emission can be tuned from 600 to 800 nm (see Figure 3a), which covers a significant region of the red and near-infrared wavelength range. Absolute quantum yields of these core/shell NCs were determined by using integrated sphere method (see Experimental Section). All the core/shell samples were purified using the method described in the Experimental Section and stored in air for 3−4 months before these PL QY measurements. Table 1 summarizes the PL properties of core and corresponding core/shell materials. The best purified sample show absolute PL QYs of nearly ∼26%, which is sufficient for many applications.

Table 1. PL Properties of $CuInSe_2$ Core and Corresponding $CuInSe_2$/ZnS Core/Shell Materials: PL Emission Peaks and PL QYs[a]

samples	PL peak (core), nm	PL peak (core−shell), nm	absolute PL QYs (core), %	absolute PL QYs (core/shell), %
S1	634	612		
S2	682	643	∼4.1	∼10.1 ± 0.2
S3	724	682	∼4.0	∼15.5 ± 0.2
S4	763	716	∼4.2	∼26.2 ± 0.2
S5	789	739	∼3.4	

[a] Absolute PL QYs of core NCs were obtained from NCs without purification. Absolute PL QYs of core/shell NCs were obtained from $CuInSe_2$/ZnS core/shell NCs after purification and stored in air. Errors on the absolute QY are from duplo measurements.

Figure 3b shows a STEM image of $CuInSe_2$/ZnS core/shell NCs obtained from the $CuInSe_2$ cores having emission peak at 720 nm. It is noted that the $CuInSe_2$/ZnS core/shell NCs are nearly monodisperse pyramidal crystals. In comparison to the core diameter of ∼3 nm (estimated from absorption spectra by comparing with calculation), the average size of core/shell NCs is ∼5 nm, indicating the shell probably consists of 3−4 ZnS atomic layers. After ZnS coating, the XRD peaks (see Figure 3c) shifted to the larger angles, close to the characteristic peaks for bulk cubic ZnS. This is similar to what is observed for CdSe/ZnS and other core/shell systems.[40] EDS characterization confirmed the presence of Zn and S elements after shell growth (see Supporting Information S6).

3.3. Optical Properties. The optical gap of $CuInSe_2$ NCs, evidenced by their absorption edge and PL emission peaks are shifted significantly compared to the bulk. The exciton binding energy is also increased due to quantum confinement effects in nanoscale systems.[42−44] Excitonic features are therefore often seen for small NCs in absorption and PL emission spectra even at room temperature. For the $CuInSe_2$ NCs, an excitonic peak in the absorption spectra appears to be obscured by line broadening.[30,32] However, in PLE spectra excitonic peaks can often be more clearly observed due to the line narrowing at the short wavelength side of the PL peak (see Supporting Information S6). 2D-PLE maps were used to characterize the $CuInSe_2$ core and $CuInSe_2$/ZnS core shell NCs (see Figure 4 and Supporting Information S7). In 2D-PLE spectra, the PL intensity variation as a function of excitation wavelength was recorded. The relative oscillator strength of excitonic states and defect states (including intrinsic and surface trap states) in the confined $CuInSe_2$ NCs can be derived from PLE spectra by looking at the landscape of the color change.[43,44] For all the samples, the oscillator strength of excitonic states is higher than that of defect states. It was also observed that the excitonic feature is more

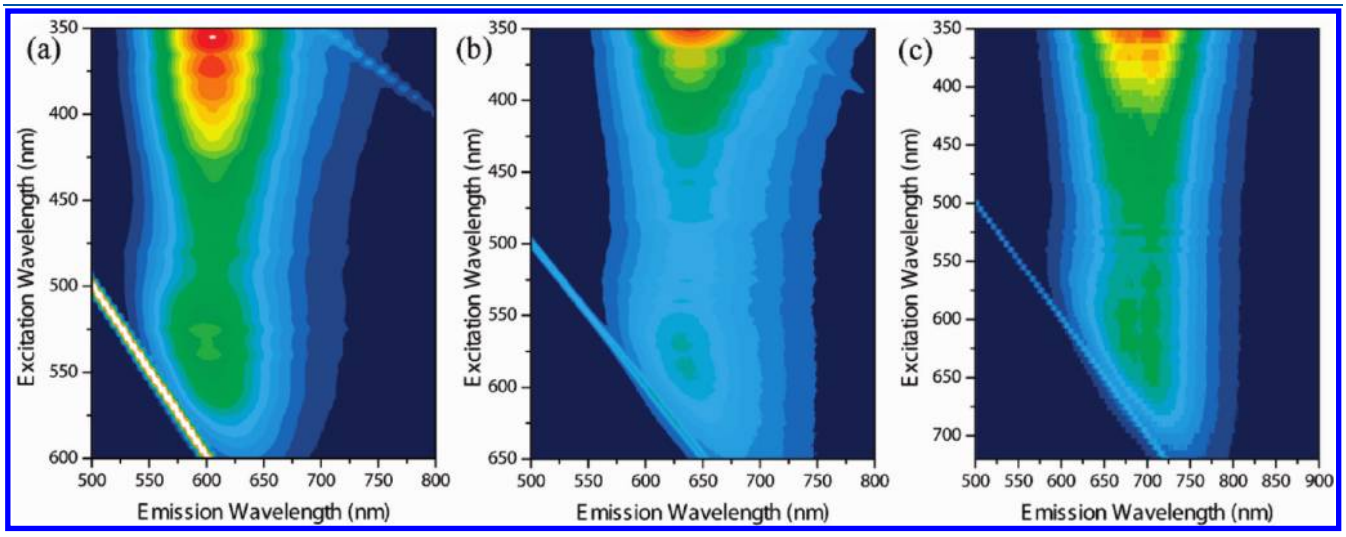

Figure 4. Typical room temperature 2D PLE spectra of colloidal $CuInSe_2$/ZnS NCs with emission peaks at wavelength of 608, 643, and 682 nm. The intensity scale (colored contours) is in arbitrary units.

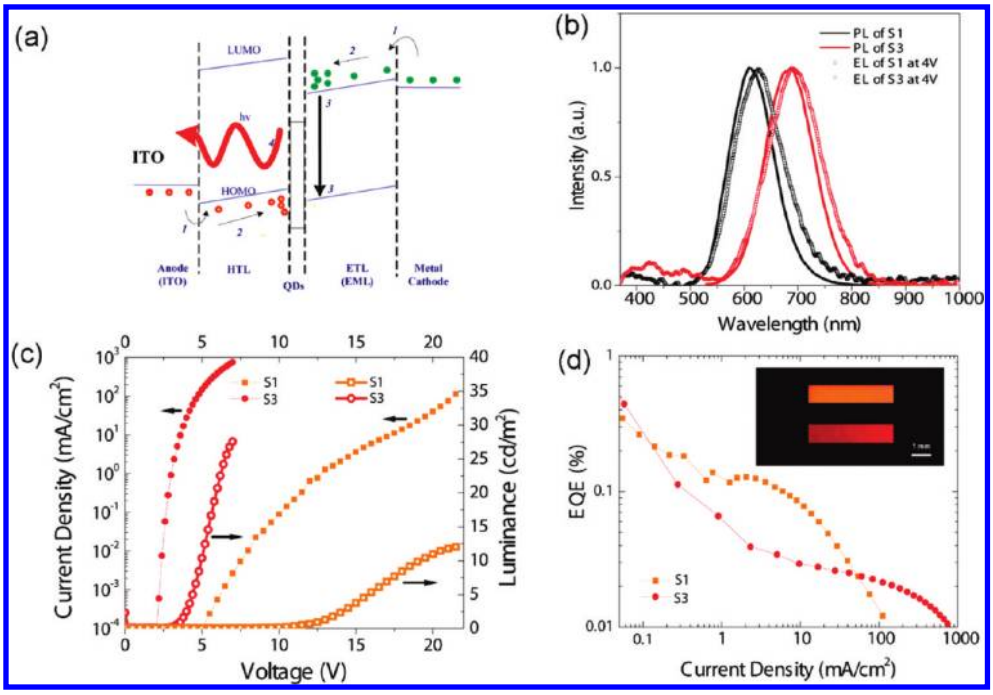

Figure 5. (a) Schematic diagram of the device structure and carrier injection. (b) The corresponding EL and PL spectra of two selected $CuInSe_2$/ZnS core/shell samples. (c) Current density and luminance of the QD-LEDs as a function of applied bias. (d) External quantum efficiency of the QD-LEDs as a function of current density; the inset on the left is the photo of the working QD-LEDs with corresponding materials displaying orange and deep-red color.

obvious for the smallest dots. Stokes shifts, the difference of optical band gap and the emission energy, were calculated to be ~280 meV for the smallest dots and gradually decreased to ~180 and ~150 meV for the larger ones, which is in consistent with the observation reported by Omata et al.[26] Consistent with these sizable Stokes shifts, the PL maps show that homogeneous line broadening (caused by exciton−phonon coupling) is significant compared to inhomogeneous line broadening (due to the particle size or composition distribution). That is concluded by comparing the spectral width antidiagonal to the line at equal emission and excitation wavelengths to the elongation along the diagonal direction. These observations suggest that a property of $CuInSe_2$ NCs is broad intrinsic line width at ambient temperature, which is probably why the excitonic band is obscured.

3.4. Light-Emitting Applications. Recently, semiconductor NCs, usually CdSe, have been combined with solution-processed organic materials, producing hybrid organic/inorganic devices for light-emitting applications.[2,3] Our preparation of highly luminescent $CuInSe_2$/ZnS core/shell NCs provides us an opportunity to test the application of these materials in LEDs.

The structure of a typical ITO/hole transport layer (HTL)/NCs/electron transport layer (ETL)/LiF/Al used to fabricate NC light-emitting diodes (QD-LED) is shown in Figure 5a. Poly(*N*,*N*-bis(4-butylphenyl)-*N*,*N*-bis(phenyl)benzidine) (poly-TPD) and 2,2′,2″-(1,3,5-benzinetriyl)tris(1-phenyl-1*H*-benzimidazole) (TPBi) were chosen as HTL and ETL layers, respectively. More details of the device fabrication and characterization are provided in the Experimental Section. The normalized EL spectra (solid lines) are shown in Figure 5b as well as their corresponding PL spectra (dashed lines) with maxima at 612 nm (S1) and 684 nm (S3). Their PL and EL spectra have similar line shapes, and a ~25 nm red shift was observed of the EL spectra in comparison to the PL emission. It is evident that ~95% of the EL comes from the NCs, although the EL spectra also show a broad, weak emission from 400 to 500 nm due to poly-TPD, TPBi, and the exciplex emission of poly-TPD/TPBi.

Figures 5c,d summarize the external quantum efficiency (EQE) of the QD-LED devices as a function of current density. The turn on voltage (V_{on}) for device with the larger dots (S3) is 2.2 V, while the V_{on} of device for smaller dots (S1) is 5.1 V. This difference may be attributed to the increasing of barrier height for charge injection in smaller dots (S1) due to their larger bandgap and/or the presence of larger amount organic capping ligands. The highest EQE of >0.3% was observed for both samples at ~0.1 cd/m^2. The maximum luminance observed was ~15 cd/m^2 (at 8 V) and ~30 cd/m^2 (at 20 V) for S1 and S3, respectively. A photo of the working QD-LEDs with a pixel size of 5 mm^2 is shown as an inset in Figure 5d, displaying uniform orange and deep red color, respectively. It is noted that the performance of $CuInSe_2$/ZnS in electroluminescence devices is lower than CdSe-based NCs.[4] The lower device efficiency may be attributed to unbalanced electron and hole injection or higher resistance of the NC layer caused by the presence of the insulating ligands.

4. CONCLUSIONS

In summary, we developed a convenient synthetic route to synthesize high quality $CuInSe_2$ NCs at a moderate reaction temperature. This method can produce $CuInSe_2$ NCs with nearly stoichiometric composition and excellent PL properties. Quantum confinement effects were observed for excitonic transitions in the $CuInSe_2$ NCs, as predicted by their small diameter (~3 nm) compared to the bulk exciton Bohr radius (10.6 nm). To explore the potential applications as light emitters, $CuInSe_2$/ZnS core shell NCs were synthesized and characterized. The PL QYs of $CuInSe_2$/ZnS core/shell NCs reached ~26% (absolute

quantum yields measured by integrated sphere) for the purified NCs solutions. We explored the application of these $CuInSe_2$/ZnS core shell materials as light emitters for electroluminescent devices. The initial results demonstrated the potential of $CuInSe_2$-based NCs as alternative materials for light-emitting applications, although the device performances need to be further improved by engineering the materials and device structures in future work. Overall, $CuInSe_2$-based NCs have potential as comparatively low toxicity luminescent quantum dots in other light-emitting applications such as white light-emitting diodes and biolabeling.[27,45,46]

■ ASSOCIATED CONTENT

Supporting Information. (1) Theoretical calculations, (2) enlarged images of $CuInSe_2$ nanocrystals, (3) EDS analysis results, (4) UV−vis absorption spectra and STEM image, (5) evolution of UV−vis and PL spectra during $CuInSe_2$/ZnS NCs growth, (6) EDS spectra of $CuInSe_2$/ZnS NCs, and (7) PLE and line-narrowed PL spectra. This material is available free of charge via the Internet at http://pubs.acs.org.

■ AUTHOR INFORMATION

Corresponding Author

*E-mail: hzzhong@bit.edu.cn (H.Z.); gscholes@chem.utoronto.ca (G.D.S.).

■ ACKNOWLEDGMENT

The Natural Sciences and Engineering Research Council of Canada is gratefully acknowledged for support of this research. This research was also supported under NFSC Research Grants (No. 51003005), National Basic Research Program of China (No. 2011CB933600), Excellent Young Scholars Research Fund of Beijing Institute of Technology (No. 2010Y0913), and the 111 research base (BIT111-201101). The authors thank N. Coombs, S. Petrov, B. Chen, Y. Ding, and Y. Li for assistance with material characterizations and Y. Zhang and J. Tang for valuable discussions and help.

■ REFERENCES

(1) Scholes, G. D. *Adv. Funct. Mater.* **2008**, *18*, 1157–1172.
(2) Rogach, A. L.; Gaponik, N.; Lupton, J. M.; Bertoni, C.; Gallardo, D. E.; Dunn, S. N.; Pira, L.; Paderi, M.; Repetto, P.; Romanov, S. G.; O'Dwyer, C.; Torres, C. M. S.; Eychmuller, A. *Angew. Chem., Int. Ed.* **2008**, *47*, 6538–6549.
(3) Rogach, A. L.; Eychmuller, A.; Hickey, S. G.; Kershaw, S. V. *Small* **2007**, *3*, 536–557.
(4) Sun, Q. J.; Wang, Y. A.; Li, L. S.; Wang, D. Y.; Zhu, T.; Xu, J.; Yang, C. H.; Li, Y. F. *Nature Photonics* **2007**, *1*, 717–722.
(5) Kamat, P. V. *J. Phys. Chem. C* **2008**, *112*, 18737–18753.
(6) Klimov, V. I.; Ivanov, S. A.; Nanda, J.; Achermann, M.; Bezel, I.; McGuire, J. A.; Piryatinski, A. *Nature* **2007**, *447*, 441–446.
(7) Konstantatos, G.; Sargent, E. H. *Nature Nanotechnol.* **2010**, *5*, 391–400.
(8) Tisdale, W. A.; Williams, K. J.; Timp, B. A.; Norris, D. J.; Aydil, E. S.; Zhu, X. Y. *Science* **2010**, *328*, 1543–1547.
(9) Sukhovatkin, V.; Hinds, S.; Brzozowski, L.; Sargent, E. H. *Science* **2009**, *324*, 1542–1544.
(10) *Nature Nanotechnol.* **2010**, *5*, 381−381.
(11) Omata, T.; Nose, K.; Otsuka-Yao-Matsuo, S. *J. Appl. Phys.* **2009**, *105*, 073106.
(12) Talapin, D. V.; Lee, J. S.; Kovalenko, M. V.; Shevchenko, E. V. *Chem. Rev.* **2010**, *110*, 389–458.
(13) Hillhouse, H. W.; Beard, M. C. *Curr. Opin. Colloid Interface Sci.* **2009**, *14*, 245–259.
(14) Castro, S. L.; Bailey, S. G.; Raffaelle, R. P.; Banger, K. K.; Hepp, A. F. *Chem. Mater.* **2003**, *15*, 3142–3147.
(15) Guo, Q. J.; Kim, S. J.; Kar, M.; Shafarman, W. N.; Birkmire, R. W.; Stach, E. A.; Agrawal, R.; Hillhouse, H. W. *Nano Lett.* **2008**, *8*, 2982–2987.
(16) Panthani, M. G.; Akhavan, V.; Goodfellow, B.; Schmidtke, J. P.; Dunn, L.; Dodabalapur, A.; Barbara, P. F.; Korgel, B. A. *J. Am. Chem. Soc.* **2008**, *130*, 16770–16777.
(17) Zhong, H. Z.; Li, Y. C.; Ye, M. F.; Zhu, Z. Z.; Zhou, Y.; Yang, C. H.; Li, Y. F. *Nanotechnology* **2007**, *18*, 025602.
(18) Tang, J.; Hinds, S.; Kelley, S. O.; Sargent, E. H. *Chem. Mater.* **2008**, *20*, 6906–6910.
(19) Koo, B.; Patel, R. N.; Korgel, B. A. *J. Am. Chem. Soc.* **2009**, *131*, 3134–3135.
(20) Norako, M. E.; Brutchey, R. L. *Chem. Mater.* **2010**, *22*, 1613–1615.
(21) Li, B.; Xie, Y.; Huang, J. X.; Qian, Y. T. *Adv. Mater.* **1999**, *11*, 1456–1459.
(22) Yang, Y. H.; Chen, Y. T. *J. Phys. Chem. B* **2006**, *110*, 17370–17374.
(23) Landry, C. C.; Barron, A. R. *Science* **1993**, *260*, 1653–1655.
(24) Grisaru, H.; Palchik, O.; Gedanken, A.; Palchik, V.; Slifkin, M. A.; Weiss, A. M. *Inorg. Chem.* **2003**, *42*, 7148–7155.
(25) Allen, P. M.; Bawendi, M. G. *J. Am. Chem. Soc.* **2008**, *130*, 9240–9241.
(26) Nose, K.; Omata, T.; Otsuka-Yao-Matsuo, S. *J. Phys. Chem. C* **2009**, *113*, 3460.
(27) Cassette, E.; Pons, T.; Bouet, C.; Helle, M.; Bezdetnaya, L.; Marchal, F.; Dubertret, B. *Chem. Mater.* **2010**, *22*, 6117–6124.
(28) Peng, Z. A.; Peng, X. G. *J. Am. Chem. Soc.* **2001**, *123*, 183–184.
(29) Talapin, D. V.; Haubold, S.; Rogach, A. L.; Kornowski, A.; Haase, M.; Weller, H. *J. Phys. Chem. B* **2001**, *105*, 2260–2263.
(30) Xie, R. G.; Rutherford, M.; Peng, X. G. *J. Am. Chem. Soc.* **2009**, *131*, 5691–5697.
(31) Castro, S. L.; Bailey, S. G.; Raffaelle, R. P.; Banger, K.; Hepp, A. F. *J. Phys. Chem. B* **2004**, *108*, 12429–12435.
(32) Zhong, H. Z.; Zhou, Y.; Ye, M. F.; He, Y. J.; Ye, J. P.; He, C.; Yang, C. H.; Li, Y. F. *Chem. Mater.* **2008**, *20*, 6434–6443.
(33) Zhong, H. Z.; Lo, S. S.; Mirkovic, T.; Li, Y. C.; Ding, Y. Q.; Li, Y. F.; Scholes, G. D. *ACS Nano* **2010**, *4*, 5253–5262.
(34) Guo, Q. J.; Ford, G. M.; Hillhouse, H. W.; Agrawal, R. *Nano Lett.* **2009**, *9*, 3060–3065.
(35) Tang, Z. Y.; Kotov, N. A.; Giersig, M. *Science* **2002**, *297*, 237–240.
(36) Reiss, P.; Protiere, M.; Li, L. *Small* **2009**, *5*, 154–168.
(37) Uehara, M.; Watanabe, K.; Tajiri, Y.; Nakamura, H.; Maeda, H. *J. Chem. Phys.* **2008**, *129*, 134709.
(38) Nose, K.; Soma, Y.; Omata, T.; Otsuka-Yao-Mats, S. *Chem. Mater.* **2009**, *21*, 2607–2613.
(39) Omata, T.; Nose, K.; Otsuka-Yao-Mats, S. *J. Nanosci. Nanotechnol.* **2011**, *11*, 4815–4823.
(40) Li, J. J.; Wang, Y. A.; Guo, W. Z.; Mishima, T. D.; Johnson, M. B.; Peng, X. G. *J. Am. Chem. Soc.* **2003**, *125*, 12567–12575.
(41) Mao, C. D.; Chuang, C. H.; Wang, D. W.; Burda, C. *J. Phys. Chem. C* **2011**, *115*, 8945–8954.
(42) Scholes, G. D.; Rumbles, G. *Nature Mater.* **2006**, *5*, 683–696.
(43) Babentsov, V.; Sizov, F. *Opto-Electron. Rev.* **2008**, *16*, 208–225.
(44) Zhong, H. Z.; Nagy, M.; Jones, M.; Scholes, G. D. *J. Phys. Chem. C* **2009**, *113*, 10465–10470.
(45) Dai, Q. Q.; Duty, C. E.; Hu, M. Z. *Small* **2010**, *6*, 1577–1588.
(46) Zhang, Y.; Xie, C.; Su, H. P.; Pickering, S. P.; Wang., Y. Q.; Yu, W. W.; Wang, J. K.; Wang, Y. D.; Hahm, J-I.; Dellas, N.; Mohney, S. E.; Xu, J. *Nano Lett.* **2011**, *11*, 329–332.